Applied Clay Science xxx (2016) xxx–xxx

Contents lists available at ScienceDirect

Applied Clay Science

journal homepage: www.elsevier.com/locate/clay

Research paper

# Multi-technique investigation of metakaolin and slag blended portland cement pastes

Natallia Shanahan *, Ananya Markandeya, Ahmed Elnihum, Yuri P. Stetsko, A. Zayed

*Department of Civil and Environmental Engineering, University of South Florida, 4202 E. Fowler Ave., Tampa, FL 33620, USA*

ARTICLE INFO

*Article history:*
Received 6 April 2016
Received in revised form 15 July 2016
Accepted 17 July 2016
Available online xxxx

*Keywords:*
Metakaolin
Blast furnace slag
X-ray diffraction
Nitrogen adsorption
Porosity
Nanoindentation

ABSTRACT

Increasing incorporation of metakaolin (MK) into field concrete mixtures necessitates careful study of the portland cement/MK hydrating systems. While a number of studies have been conducted on MK blends with cement, the current knowledge on its effect on hydration products and paste microstructure remains incomplete. This study evaluated the effect of MK on the nature of hydration products through X-ray diffraction, while the effect on microstructure was assessed by measuring porosity with nitrogen adsorption and determining nanoindentation modulus as well as volume fractions of CSH with varying packing densities. The 10MK paste hydrated for 7 days was compared to the plain ordinary portland cement (OPC) paste as well as to paste containing 52% slag (52SL). No significant effect was observed on the nature of hydration products with MK or SL addition. However, nitrogen-accessible porosity increased with MK and SL addition, the increase being larger with SL. The average indentation modulus for hydration products decreased with addition of MK and SL which corresponded to increasing nitrogen accessible pores.



## 1. Introduction

Metakaolin (MK) is a relatively new supplementary cementitious material (SCM) that has been introduced in the 1990s (Ramezanianpour, 2014). MK is a pozzolanic material obtained by subjecting kaolin to heat treatment (calcination) at 500–800 °C. Upon heating, kaolinite ($SiO_2 \cdot 2Al_2O_3 \cdot 2H_2O$) is dehydroxylated and transformed into a more disordered metakaolin phase (Shvarzman et al., 2003). MK generally consists of 50% $SiO_2$ and 40% $Al_2O_3$, although its exact composition varies depending on the source of kaolin clay (Ramlochan et al., 2000; Kakali et al., 2001; Shvarzman et al., 2003; Bich et al., 2009). Incorporation of MK into concrete has been gaining popularity due to the increase in early compressive strength and reduced permeability (Gruber et al., 2001; Justice et al., 2005; Poon et al., 2006; Duan et al., 2013). MK is typically added to concrete at cement replacement level of 10% in order to maximize compressive strength (Ambroise et al., 1994; Poon et al., 2001; Batis et al., 2005). It has been established that maximum contribution of MK to compressive strength occurs at approximately 14 days, after which the pozzolanic reaction of MK slows down (Wild et al., 1996; Ramezanianpour, 2014). Therefore, early-age properties of the OPC/MK mixtures are of particular interest in studying the effect of MK.

While the effect of metakaolin on hardened concrete properties has been the topic of a large number of studies, its effect on the paste microstructure has not been explored in as much detail. Incorporation of MK is known to alter the chemical composition of CSH (Ambroise et al., 1994; Richardson, 2004), which is the main hydration product and is primarily responsible for concrete compressive strength. This change in CSH composition implies a possible change in its microstructure and mechanical response. Recently, Rodriguez et al. (2015) demonstrated that the CSH morphology changes from fibrillar to foil-like as the Ca/Si ratio decreases from 1.63 to 1.33. Several molecular simulations showed a change in the mechanical properties of CSH with the change in Ca/Si ratio (Abdolhosseini Qomi et al., 2014; Bauchy et al., 2014; Hou et al., 2015).

Nanoindentation has been extensively used to ascertain the mechanical properties of CSH, which is the main hydration product and is primarily responsible for concrete compressive strength. It has been established that the mechanical response of CSH depends on the packing density of CSH globules (Constantinides and Ulm, 2007; Ulm et al., 2007; Ulm et al., 2010; Ioannidou et al., 2016). Values of elastic moduli have been published for a number of CSH morphologies which are summarized in Table 1. There exists a very porous phase, the elastic modulus of which is affected by capillary porosity (Constantinides and Ulm, 2007; Mondal et al., 2010; Hu et al., 2014), with a modulus of approximately 8–13 GPa, low-density or outer product CSH with an elastic modulus ≈ 21 GPa, high-density or inner product CSH with a modulus ≈ 30 GPa, and CH or a mixture of CSH and CH also referred to as ultra-high-density CSH with a modulus of 36–40 GPa.

While nanoindentation has been applied to $C_3S$ and OPC pastes, there are few studies on nanoindentation of OPC/MK samples. He et

* Corresponding author.
*E-mail address:* nkashalo@mail.usf.edu (N. Shanahan).

http://dx.doi.org/10.1016/j.clay.2016.07.015
0169-1317/

**Table 1**
Summary of published elastic moduli values for CSH and CH.

| Phase | Mean ± standard deviation (GPa) | Reference |
|---|---|---|
| Low stiffness phase | 8.1 | Constantinides and Ulm (2007) |
| Porous phase | 9.4 ± 3.4 | Mondal et al. (2010) |
| Very porous (VP) CSH | 13.6 ± 1.0 | Hu et al. (2014) |
| Low stiffness CSH | 16.5 ± 4.7 | Mondal et al. (2010) |
| | 22.89 ± 0.76 | Mondal et al. (2007) |
| Low-density (LD) CSH | 18.2 ± 4.2 | Constantinides and Ulm (2007) |
| | 21.7 ± 2.2 | Constantinides and Ulm (2004) |
| | 22.39 ± 4.84 | Vandamme and Ulm (2013) |
| | 22.5 ± 5.0 | Vandamme et al. (2010) |
| Outer product (OP) CSH | 20.8 ± 3.2 | Hu et al. (2014) |
| Medium stiffness CSH | 31.16 ± 2.51 | Mondal et al. (2007) |
| High stiffness CSH | 27.1 ± 3.5 | Mondal et al. (2010) |
| | 41.45 ± 1.75 | Mondal et al. (2007) |
| High-density (HD) CSH | 29.1 ± 4.0 | Constantinides and Ulm (2007) |
| | 29.4 ± 2.4 | Constantinides and Ulm (2004) |
| | 30.4 ± 2.9 | Vandamme et al. (2010) |
| | 34.82 ± 5.25 | Vandamme and Ulm (2013) |
| Inner product (IP) CSH | 31.0 ± 3.1 | Hu et al. (2014) |
| Ultra-high-density (UHD) CSH | 40.9 ± 7.7 | Vandamme et al. (2010) |
| CH | 40.3 ± 4.2 | Constantinides and Ulm (2007) |
| | 36.9 ± 3.5 | Mondal et al. (2010) |
| | 38 ± 5.0 | Constantinides and Ulm (2004) |
| | 39.77–44.89 | Monteiro and Chang (1995) |

al. (2013) investigated the effect of SCM, including MK, on the elastic moduli of the hydration products and the volume fractions of LD and HD CSH. Samples containing SCM were prepared with a water to binder (w/b) ratio of 0.3, while the control sample had a w/b ratio of 0.35 in order to obtain similar 28-day compressive strengths. The authors reported that at the age of 60 days the control sample had the smallest fraction of HD CSH, while for the samples containing SCM the HD CSH fraction appeared to increase with an increase in the molar fraction of (Al + Si)/Ca in the OPC-SCM blend. However, the control sample did not fit this relationship, possibly due to a difference in the w/b ratio. The authors concluded that the (Al + Si)/Ca ratio can be used in place of nanoindentation tests for cementitious mixtures with the same w/b ratio and similar 28-day compressive strengths in order to predict the fraction of HD CSH. Only two types of CSH, LD and HD, were observed in this study, with no significant difference in their values regardless of SCM addition.

Barbhuiya and Chow (2015) reported nanoindentation modulus and hardness values for PC and PC + 10%MK pastes. The calculated volume fractions of LD and HD CSH (≈36% each) in the PC + 10%MK sample were only slightly higher than those of the PC sample (≈33% for each). However, the age or degree of hydration of the samples was not reported, and it remains unclear whether these results are indicative of early-age or later-age characteristics on the MK-containing pastes.

In addition to a change in CSH composition, a change in porosity with MK addition has been reported as well. Ambroise et al. (1994) reported an increased amount of pores in the 6–20 nm range with 20–30% MK addition. Poon et al. (2001) also reported that addition of metakaolin at a constant w/cm ratio decreases the average pore diameter for any age and at any cement replacement level up to 20%.

The effect of chemical and mineral admixtures on pore size distribution is of great interest as pores of different sizes will have an impact on different concrete properties. Juenger and Jennings (2002) observed that an increase in the nitrogen accessible pore volume and surface area corresponded to increased drying shrinkage. Jennings et al. (2008) also stated that creep is affected by gel porosity.

Porosity of the OPC/MK mixtures has been predominantly studied using mercury intrusion porosimetry (MIP) (Ambroise et al., 1994; Duan et al., 2012, 2013; Khatib and Wild, 1996; Poon et al., 2001, 2006). Although MIP can measure a wide range of pore sizes from approximately 2 nm to 100 μm (Aligizaki, 2006), this technique measures the pore entry sizes rather than the actual pore diameters. Nitrogen ($N_2$) adsorption is another technique that can be used to measure porosity although it is limited predominantly to the mesopore range. However, unlike MIP, it is not affected by pore network effects when the adsorption branch is used (Aligizaki, 2006). The study by Justice and Kurtis (2007) is the only study to date that utilized nitrogen adsorption to measure porosity of the OPC/MK samples. However, the authors reported only percent of total pore volume for pores < 10 nm, 10–20 nm and >20 nm diameters, which provides limited information on how pore size distributions compare between plain OPC samples and those containing MK. No information was found on the effect of SL incorporation on porosity as measured by $N_2$ adsorption.

The goal of this study was to investigate the effect of cement replacement with 10%MK on the hydration products, nanoindentation characteristics and porosity at the age of 7 days and compare the effect of MK to that of SL as well as to the plain OPC paste at ambient temperature using cement replacement dosages and chemical admixtures that are typically used in structural concrete. Additionally, since nanoindentation modulus depends on CSH packing density and packing density determines CSH porosity, a possible relationship between nanoindentation modulus and porosity was investigated as well.

## 2. Methodology

### 2.1. As-received materials characterization

A Type I/II commercial Portland cement and two SCM, metakaolin (MK) and blast furnace slag (SL) were selected for this study. Detailed characterization of these materials was described by Zayed et al. (2016). X-ray fluorescence spectroscopy (XRF) was used to determine the chemical oxide composition of cement, MK and SL in accordance with ASTM C114.

Mineralogical composition of the cementitious materials was determined from X-ray diffraction (XRD) measurements following ASTM C1365. Prior to XRD measurements, cement was wet-ground in ethanol in a McCrone micronizing mill to a particle size between 1 and 10 μm. The wet grinding method was used to avoid the effect of temperature on gypsum and its possible phase transformation to hemihydrate or anhydrite. The samples were then dried in an oven at 43 °C. MK and SL samples were mixed with a standard reference material, (SRM) 676a, obtained from the National Institute of Standards and Technology (NIST). SRM 676a was used as an internal standard (IS) in order to determine the amorphous unidentified content of each sample (Madsen et al., 2011). Since MK and SL are known to be predominantly amorphous (Mindess et al., 2003), the internal standard was used at 10% replacement level, which was shown to be optimal for samples with amorphous content of around 90% (Westphal et al., 2009).

XRD measurements were performed using the Phillips X'Pert PW3040 Pro diffractometer equipped with the X'Celerator Scientific detector and a Cu-Kα X-ray source (λ = 1.540598 Å). Tension and current were set to 45 kV and 40 mA respectively. Scans were performed in the range of 7–70° 2θ, with a step size of 0.0167° 2θ and a counting time per step of 130.2. 5 mm divergence and anti-scatter slits were used in the automatic mode. Samples were loaded into the sample holder using a back-loading technique in order to minimize preferred orientation, and placed onto a spinner stage that was rotating at 30 rpm in order to improve counting statistics (Bish and Reynolds, 1989). Mineralogical

Please cite this article as: Shanahan, N., et al., Multi-technique investigation of metakaolin and slag blended portland cement pastes, Appl. Clay Sci. (2016), http://dx.doi.org/10.1016/j.clay.2016.07.015

analysis of the collected diffraction patterns was carried out using Panalytical HighScore Plus 3.0 software. Quantification was performed using the Rietveld refinement functionality built into the software. Chebyshev II function was used to calculate the background, and Pseudo Voigt function was used for profile fitting. Crystallographic parameters for cement and SCM are included in the Appendix (Tables 1A–3A).

Particle size distribution (PSD) of cement, MK and SL was measured using an LA-950 particle size analyzer manufactured by HORIBA Instruments using the dry method. Triplicate tests were conducted on all materials and the average results are reported here (Table 4 and Fig. 1). In addition to PSD, fineness of all the materials was determined by nitrogen adsorption using Autosorb-1 analyzer manufactured by Quantachrome Instruments. The samples were outgassed under vacuum at 80 °C immediately prior to analysis in order to remove any moisture or contaminants from the sample surface. The Brunauer-Emmett-Teller (BET) method (Brunauer et al., 1938) was used for the specific surface area (SSA) calculations. Multipoint BET was selected over the single point BET for greater accuracy (Aligizaki, 2006).

Additionally, four chemical admixtures that are commonly used in structural concrete mixtures, air-entraining admixture (AEA), water-reducing and retarding admixture (WRRA) and two superplasticizers (SP), were used. According to the manufacturer's safety data sheets, WRRA was lignosulfonate-based and both SP1 and SP2 were polyacrylate-based with SP1 being more concentrated. In the field, SP1 is used in concrete containing MK, while SP2 is used with SL. Since MK is expected to be finer than SL, a more concentrated SP is needed to achieve proper particle dispersion with the incorporation of MK.

### 2.2. Paste characterization

#### 2.2.1. Isothermal calorimetry

Table 2 lists the paste mix designs used in this study. A constant w/cm ratio of 0.485 was used for all the mixtures taking into account the water added as part of the chemical admixtures. Heat of hydration of the mixtures was measured using TAM Air 8-twin channel isothermal calorimeter manufactured by TA Instruments. The measurements were performed at 23 °C following the ASTM C1702 Method A, internal mixing.

The degree of hydration, $\alpha(t)$, for each mixture was calculated based on isothermal calorimetry measurements. $\alpha(t)$ was calculated following Eq. (1):

$$\alpha(t) = \frac{H(t)}{H_u} \tag{1}$$

where $H(t)$ is the total heat released by each mixture at time $(t)$ and $H_u$ is the total available heat that can be generated by the cementitious components of the mixture at complete hydration. For pastes without SCM, $H_u = H_{cem}$.

$$H_{cem} = 500P_{C3S} + 260P_{C2S} + 866P_{C3A} + 420P_{C4AF} + 624P_{SO3} + 1186P_{FreeCaO} + 850P_{MgO} \tag{2}$$

where $H_{cem}$ is the total heat of hydration of portland cement and $P_i$ is the mass of $i$th component to total cement content ratio. For the 52SL sample, $H_u$ was calculated using the equation provided by (Schindler and Folliard, 2005), but eliminating the fly ash contribution:

$$H_u = H_{cem}P_{cem} + 461P_{slag} \tag{3}$$

The current models proposed in the literature to predict hydration behavior of OPC/SCM systems (Poole et al., 2007; Riding et al., 2012; Schindler and Folliard, 2005) do not include metakaolin. The only guidance regarding the heat of hydration (HOH) of MK mixtures comes from Gajda (2007) who states that it can be approximated as "100% to 125% that of Portland cement." For the 10MK mix, $H_u$ was calculated using the upper limit proposed by Gajda (2007):

$$H_u = H_{cem}P_{cem} + 1.25H_{cem}P_{MK} \tag{4}$$

Riding et al. (2012) showed that chemical admixtures affect the rate of heat evolution as well as the ultimate degree of hydration ($\alpha_u$). However, they do not affect $H_u$, since it is the heat that could potentially be generated at complete hydration of the cementitious materials and is a function of cement chemistry as well as the amount and type of SCM present (Schindler and Folliard, 2005).

#### 2.2.2. Sample preparation for X-ray diffraction, nanoindentation and nitrogen adsorption

Samples were mixed using the IKA WERKE mixer. The WRRA was added to the mixing water; AEA was introduced after mixing for 1 min at 300 rpm, which was followed by 30 s of mixing at 600 rpm. Superplasticizer (SP1 or SP2) was added after a 90 second rest period, after which the paste was mixed for an additional 60 s at 600 rpm. After mixing, paste samples were sealed and cured under isothermal conditions at 23 °C.

#### 2.2.3. X-ray diffraction and Rietveld analysis of hydrated pastes

For X-ray diffraction (XRD), demolded samples were ground by hand with an agate mortar and pestle. Paste samples were mixed SRM 676a in order to determine the amorphous/unidentified content of each sample (Madsen et al., 2011). Since the amorphous/unidentified content of the hydrated pastes was expected to be lower compared to the as-received SCM, the internal standard was used at 20% replacement as recommended by Westphal et al. (2009). SRM 676a was mixed with the paste by hand with the mortar and pestle in order to avoid increasing the amorphous content of the paste during grinding (Jansen et al., 2011a, 2011b, 2012). No specific technique was used to stop the hydration, as samples were prepared immediately after demolding and loaded into the diffractometer. XRD measurements were conducted in the same manner as described previously for the as-received materials in Section 2.1.

#### 2.2.4. Nitrogen adsorption

Samples for porosity measurement by nitrogen adsorption were mixed and cured as described in Section 2.2.2 until the age of 7 days at 23 °C. Immediately after demolding, the samples were crushed and sieved to separate the particles in the range of 1–3 mm, and dried at 105 °C under vacuum for 2 h using the outgasser built into Autosorb-1 analyzer. This drying procedure was selected as drying at a lower temperature may accelerate the hydration process (Korpa and Trettin, 2006) and is not suitable at early ages. Slow removal of water by procedures such as D-drying does not quickly arrest the hydration (Aligizaki, 2006). Drying at 105 °C was limited to 2 h to avoid damaging the CSH microstructure, which is typically a concern with drying at this temperature for 24 h (Detwiler et al., 2001). Beaudoin (2002) suggests that limiting oven-drying at 105 °C to 2–3 h results in a microstructure that is similar to D-drying, which would be most suitable for nitrogen adsorption. In this work, samples were dried for 2 h, after which nitrogen isotherms were collected using Autosorb-1.

Pore size distribution calculations were performed using the Barrett, Joyner, Halenda (BJH) method (Barrett et al., 1951), adsorption branch. Since the adsorption branch measures the size of the interior of the pore it was selected over the desorption branch, which measures the pore entry size (Bodor et al., 1970; Scherer, 2015). Additionally, the adsorption branch is not influenced by the pore network effects to the same degree as the desorption branch (Bodor et al., 1970; Groen et al., 2003). Brunauer, Emmett, Teller (BET) method (Brunauer et al., 1938) was used to calculate the specific surface area, which is typically attributed to CSH (Gluth and Hillemeier, 2012).

Please cite this article as: Shanahan, N., et al., Multi-technique investigation of metakaolin and slag blended portland cement pastes, Appl. Clay Sci. (2016), http://dx.doi.org/10.1016/j.clay.2016.07.015

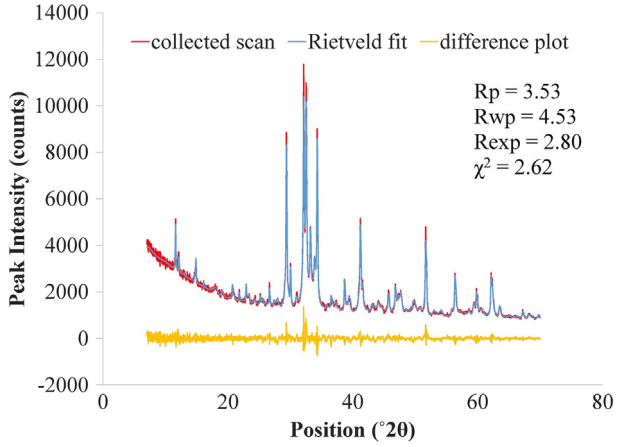


**Fig. 1.** XRD scan and the Rietveld fitted profile for the as-received cement sample.

*2.2.5. Nanoindentation*

Nanoindentation samples were demolded at the age of 7 days, crushed and placed in isopropanol for 48 h to stop hydration. After 48 h, the samples were dried under vacuum and cast in SPECIFIX-40 two part epoxy from Struers. Samples were polished using MD-Piano series polishing discs #200, 500, 1200, followed by diamond suspensions of 3, 1, and 0.25 μm. The diamond suspensions were used with MD-Dur polishing cloths. As a final step, the samples were polished with 0.5 alumina powder suspension on an MD-Nap polishing cloth. Samples were washed in ethanol in an ultrasonic bath for 10 min between each polishing step.

Indentation measurements were performed using the Hysitron Ti 900 Triboindenter with a Berkovich tip. A trapezoidal loading function was used with a 5 second loading time, 3 second hold period and a 5 second unloading period and a maximum load ($P_{max}$) of 2 mN. Instrument compliance and tip area function calibrations were performed using a fused quartz standard prior to sample measurements. A minimum of 50 points were indented for each sample. Constantinides and Ulm (2007) showed that 50 nanoindentation points were sufficient to identify correct volume fractions of HD and LD CSH and no further improvement was achieved by increasing the number of indentations. Points were indented in a grid of 10 × 10 points, spaced 20 μm apart.

The data were analyzed based on the Oliver and Pharr method (Oliver and Pharr, 1992) using the TriboScan 6.0 software. After analyzing the indentation results, the data was normalized by the number of indents in each sample and deconvoluted to obtain the modulus of individual phases as described in Constantinides et al. (2006).

## 3. Results and discussion

### 3.1. Materials characterization

Table 3 lists the results of the chemical oxide analysis. Cement selected for this study had a low equivalent alkali content ($Na_2O_{eq}$) and so did the MK and SL. The oxide composition of MK used in this study is in general agreement with the published values except for its lower $Fe_2O_3$ content (Buchwald et al., 2009; Curcio et al., 1998; Siddique and Khan, 2011). The oxide composition of slag is also in general agreement with the values found in the literature, except for a higher $Al_2O_3$ content than is typically used in cement mixtures (Boháč et al., 2014; Richardson and Groves, 1992; Riding et al., 2012).

**Table 2**
Mixture proportions.

| Sample | Mineral admixture | Mineral admixture (% cement replacement) | WRRA dosage | AEA dosage | SP2 dosage | SP1 dosage |
|---|---|---|---|---|---|---|
| | | | (ml/100 kg cementitious) | | | |
| CNSP1 | None | 0 | 110 | 2.5 | 0 | 155 |
| 10MK | Metakaolin | 10 | 110 | 2.5 | 0 | 155 |
| 52SL | Blast furnace slag | 52 | 110 | 2.5 | 110 | 0 |

**Table 3**
Oxide chemical analysis for as-received cement and mineral admixtures.

| Analyte | Cement (wt%) | MK (wt%) | SL (wt%) |
|---|---|---|---|
| $SiO_2$ | 20.40 | 51.29 | 35.15 |
| $Al_2O_3$ | 5.20 | 44.16 | 14.25 |
| $Fe_2O_3$ | 3.20 | 0.49 | 0.48 |
| CaO | 63.10 | <0.01 | 41.45 |
| MgO | 0.80 | 0.14 | 5.21 |
| $SO_3$ | 3.60 | <0.01 | 1.86 |
| $Na_2O$ | 0.10 | 0.26 | 0.22 |
| $K_2O$ | 0.38 | 0.27 | 0.32 |
| Total | 100.10 | 99.22 | 99.83 |
| $Na_2O_{eq}$ | 0.35 | 0.44 | 0.43 |

X-ray diffractograms and fitted Rietveld profiles for cement, MK and SL are presented in Figs. 1–3. The quality of Rietveld analysis can evaluated through the use of statistical parameters, such as Rwp (weighted profile residual) or $\chi^2$ (goodness of fit) (Pecharsky et al., 2009), as well as visually, by inspecting the difference between the collected data and the fitted profile. Both statistical parameters and the difference plots are included in the figures.

Rwp and $\chi^2$ have been used in the published literature to evaluate the quality of Rietveld analysis. Toby (2012) states that for a well-fitted profile, $\chi^2$ value should be close to, but >1. At the same time, he acknowledges, that simply using longer counting times during data collection can increase $\chi^2$. Kniess et al. (2012) state that values of Rwp in the range of 2–10 are indicative of a good refinement. For MK and SL, $\chi^2$ values were lower than that of cement and very close to 1, most likely due to the large contribution of the background to the diffraction patterns (Toby, 2012). The $\chi^2$ value for cement is consistent with the published literature (Peterson et al., 2006). Rwp values for all the materials were within the range specified by Kniess et al. (2012). The quality of fit was further confirmed by visual inspection.

Mineralogical composition of cement and SCMs is listed in Table 4. As expected, both MK and SL had high amorphous content. High amorphous content is necessary for the use of these materials in concrete production as crystalline phases are non-reactive and do not contribute to improvement of concrete properties.

Particle size analysis showed that SL had a very similar BET SSA and particle size distribution to that of cement, while MK was much finer (Table 5 and Fig. 4).

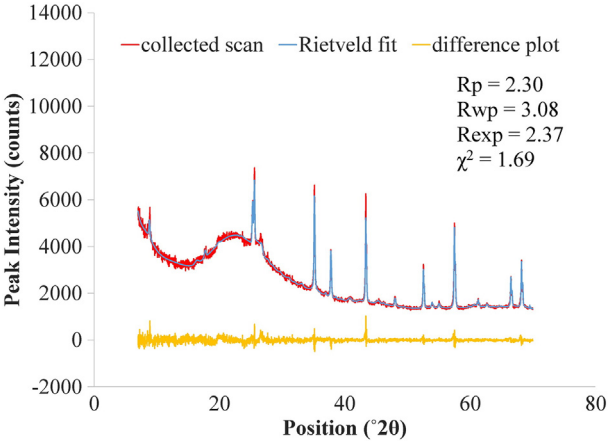


**Fig. 2.** XRD scan and the Rietveld fitted profile for the as-received MK sample with 10% SRM 676a.

Please cite this article as: Shanahan, N., et al., Multi-technique investigation of metakaolin and slag blended portland cement pastes, Appl. Clay Sci. (2016), http://dx.doi.org/10.1016/j.clay.2016.07.015

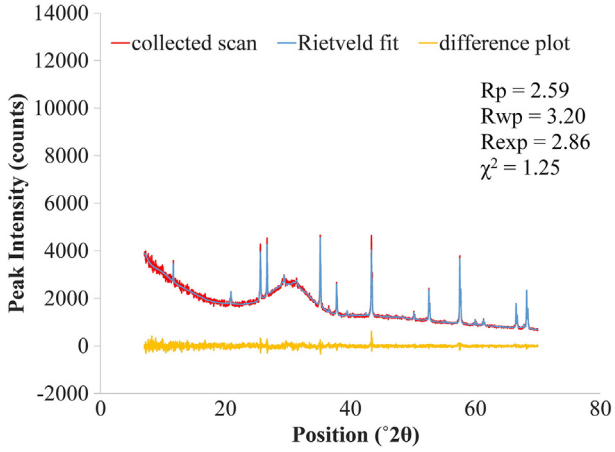


**Fig. 3.** XRD scan and the Rietveld fitted profile of the as-received SL sample with 10% SRM 676a.

### 3.2. Isothermal calorimetry

The degree of hydration for each of the paste samples (Table 6) obtained from isothermal calorimetry (Fig. 5) was calculated at the age of 7 days using Eqs. (1)–4(). As expected, the higher substitution of cement by slag shows the lowest total heat at 7 days of hydration while the total heat for 10MK and CN are similar.

### 3.3. Hydration products

Figs. 6–8 present collected diffractograms and the fitted Rietveld profiles for CN + SP1, 10MK and 52SL pastes, respectively. Rwp values for all the samples were below 10, which indicates a good fit (Kniess et al., 2012; Wilson, 2013), and are consistent with those previously published for hydrated cement pastes (Snellings, 2016).

The main crystalline hydration phases identified in the control sample at the age of 7 days were calcium hydroxide (CH), ettringite and hemicarboaluminate (Table 7). The presence of hemicarboaluminate is attributed to the reaction of tricalcium aluminate ($C_3A$) and CH with limestone, which was present in the cement used in this study. Examination of the as-received cement revealed the presence of 2.0% calcite, which is consistent with the limestone addition reported on the mill certificate for this cement. Limestone powder has been reported to react with $C_3A$ during cement hydration forming hemicarboaluminate ($C_4AC_{0.5}H_{12}$) and with $C_3A$ and CH forming monocarboaluminate ($C_4ACH_{11}$) as shown by De Weerdt et al. (2011).

**Table 4**
Mineralogical composition of cement, MK and SL.

| Analyzed sample | Phase | ICSD # | Phase content (w/o) |
|---|---|---|---|
| Cement | Alite | 94742 | 46.9 |
| | Belite | 81096 | 25.2 |
| | $C_3A$ | 1841 | 9.6 |
| | $C_4AF$ | 9197 | 8.0 |
| | Gypsum | 151692 | 2.8 |
| | Hemihydrate | 79528 | 1.8 |
| | Anhydrite | 40043 | 0.5 |
| | Calcite | 80869 | 2.0 |
| | Portlandite | 15471 | 2.5 |
| | Quartz | 41414 | 0.8 |
| Metakaolin | Illite | 90144 | 1.6 |
| | Mullite | 28544 | 1.2 |
| | Anatase | 63711 | 0.8 |
| | Amorphous | | 96.4 |
| Slag | Melilite | 158172 | 1.2 |
| | Quartz | 41414 | 1.3 |
| | Gypsum | 151692 | 0.4 |
| | Calcite | 80869 | 0.4 |
| | Amorphous | | 96.7 |

**Table 5**
Particle size analysis of as-received cement and SCMs.

| Physical properties | Cement | MK | SL |
|---|---|---|---|
| $D_{10}$ (μm) | 3.0 | 1.7 | 3.3 |
| $D_{50}$ (μm) | 13.0 | 5.5 | 10.9 |
| $D_{90}$ (μm) | 29.3 | 11.7 | 23.4 |
| Median size (μm) | 13.0 | 5.5 | 10.9 |
| Mean size (MPS) (μm) | 15.1 | 6.2 | 12.6 |
| Multipoint BET SSA ($m^2$/kg) | 2140 | 14,970 | 3700 |

In addition to the crystalline hydration products, cement reaction with water produces CSH, which has been estimated to comprise 60% of the hydration products volume (Mehta and Monteiro, 2006). CSH is a poorly crystalline phase with short range order and no known crystal structure (Mindess et al., 2003; Taylor, 1997; Van Damme et al., 2013). Although the amorphous/unidentified content of the paste cannot be solely attributed to CSH, due to the possible presence of small quantities of minor phases that could not be identified during the analysis, its presence has to be taken into consideration during Rietveld analysis. Failure to account for the presence of amorphous/unidentified content in the sample would lead to large overestimation of the crystalline hydration products.

There is a number of publications detailing the hydration products in the OPC/MK systems (Antoni et al., 2012; Boháč et al., 2014; Cassagnabère et al., 2009; Snellings et al., 2014). However, these studies have not attempted to quantify the hydration phases; therefore, our results can only be compared qualitatively. In the current study, only hemicarboaluminate was identified in the 10MK sample as opposed to the results obtained by Antoni et al. (2012), who reported the presence of both hemi- and monocarboaluminate, most likely due to significantly lower $CaCO_3$ content in the as-received cement (2.1%) compared to that used by Antoni et al. (2012) (15%).

Addition of mineral admixtures did not appear to change the main hydration products. Generally, no significant effect on phase consumption (Table 8) was observed with addition of mineral admixtures, except in the case of 52SL, where consumption of all phases was increased, likely due to the small amount of cement present in this mixture and a much higher effective w/c ratio.

### 3.4. Porosity measurement with nitrogen adsorption

Nitrogen-accessible porosity increased with addition of MK and SL (Fig. 9). This can be attributed to two factors: lower degree of hydration and changes in porosity of CSH. While the degree of hydration (Table 6)

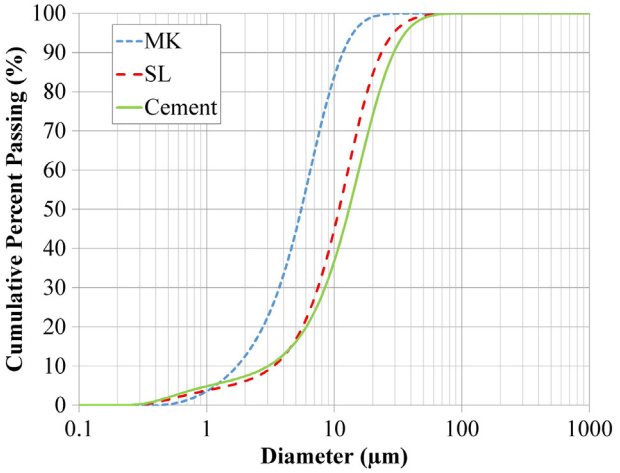


**Fig. 4.** Cumulative particle size distribution.

Please cite this article as: Shanahan, N., et al., Multi-technique investigation of metakaolin and slag blended portland cement pastes, Appl. Clay Sci. (2016), http://dx.doi.org/10.1016/j.clay.2016.07.015

**Table 6**
Degree of hydration calculated from isothermal calorimetry at the age of 7 days.

| Mix ID | Degree of hydration |
|---|---|
| CN + SP1 | 0.72 |
| 10MK | 0.68 |
| 52SL | 0.46 |

of the 52SL sample is significantly lower than that of CN + SP1 and a higher amount of LD CSH is expected at lower degrees of hydration, the degree of hydration of 10MK and CN + SP1 are similar, so the observed differences in the pore size distributions in the 1.5–10 nm range of CN + SP1 and 10MK samples are likely due to the changes in the porosity of CSH, possibly due to the changes in its chemical composition.

The measured pore size distribution for the CN + SP1 sample is in general agreement with the data published in the literature (Hemalatha et al., 2015; Mikhail et al., 1964; Shanahan et al., 2016). As for 10MK paste, it is difficult to compare the obtained results to previous studies. The study by Justice and Kurtis (2007), who used $N_2$ adsorption to measure porosity, reported % pore volumes rather than actual volumes for pore diameters below 10 nm, 10–20 nm and above 20 nm at 1 and 28 days. The rest of the studies utilized MIP, reporting the total pore volume and break through diameters, which cannot be related to the $N_2$ adsorption data. Even so, the results are contradictory. Poon et al. (2001, 2006) and Duan et al. (2013) reported lower total porosity compared to the control in 10%MK mixtures at 7 days, while Khatib and Wild (1996) observed an increase in the total pore volume at 7 days with 10% cement replacement with MK. Additionally, Khatib and Wild (1996) reported that the percentage of pores with radii < 20 nm was greater in the 10%MK sample than in the control at all ages, while the amount of pores with radii > 20 nm was always lower. The higher total pore volume of the 10MK sample compared to the control is in agreement with the findings by Khatib and Wild (1996). Since no information was found on the effect of SL incorporation on $N_2$-accessible porosity, it was not possible to compare the results obtained for 52SL paste to previous studies.

Several pore size classifications have been proposed for concrete (Aligizaki, 2006). In this study, CM-II model (Jennings, 2008) was predominantly used to separate pore size distribution into specific pore volumes. The CM-II model distinguishes two types of CSH pores: small gel pores (SGP) representing the space within CSH particles and large gel pores (LGP) between the CSH particles. It estimates the size of SGPs to be below 3 nm, and the size of LGPs to be in the range of 3–12 nm. In a recent NMR study, Valori et al. (2013) reported 10 nm pores between CSH particles. Korb et al. (2007) reported clustering of

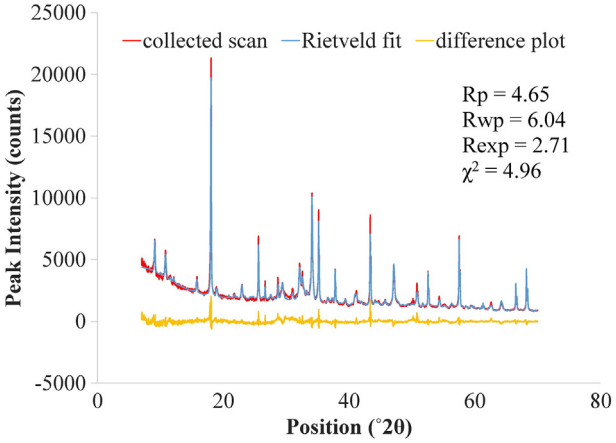


**Fig. 6.** CN + SP1 paste sample at 7 days with 20% SRM 676a.

pores around the following average values: 1.8, 7, 50 and 600 nm. The authors attributed 1.8 nm pores to the pores inside CSH (SGP pores proposed by (Jennings, 2008)) and 7 nm pores to the pores between CSH particles. Reconciling these studies as well as the pore size classification proposed by Mindess et al. (2003), pore size distributions of the samples analyzed in this study were compared for the following pore ranges: <3 nm (SGP pores), 3–10 nm (LGP pores) and >10 nm (fraction of capillary pores measured by $N_2$ sorption) (Fig. 4).

No significant differences were observed in the SGP pore volumes of the samples (Fig. 10). The LGP porosity, however, increased with the addition of SCM and was the highest for the 52SL sample. This indicates that 52SL paste had the highest LD/HD CSH ratio, which could be attributed to the lower degree of hydration of this sample. Although lower than that of 52SL, the LD/HD ratio for the 10MK sample was also notably higher than that of the control paste, in spite of their similar degree of hydration.

BET predominantly measures porosity of CSH, and there is a general agreement in the literature that $N_2$ molecules can enter the pores of low-density (LD) CSH, but only a small fraction of the high-density (HD) CSH porosity, while water can enter the pores of both LD and HD CSH (Jennings and Thomas, 2004; Jennings, 2008; Odler, 2003). Jennings and Thomas (2004) state that because of this, $N_2$ BET surface areas are much more sensitive to the microstructural differences than those obtained with water vapor. As with the pore size distribution, the highest BET SSA was observed for the 52SL sample followed by 10MK (Table 9). This is not surprising, as these parameters are related; an increase in the LGP pore volume would increase the BET SSA. Surface area of the control sample was significantly lower implying the

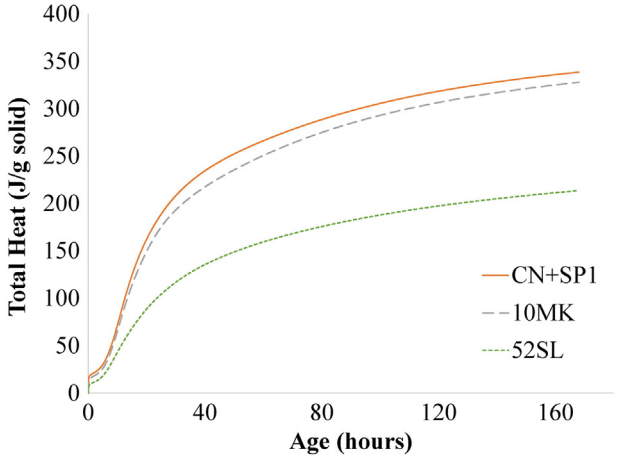


**Fig. 5.** Total heat evolved for cement and cementitious paste.

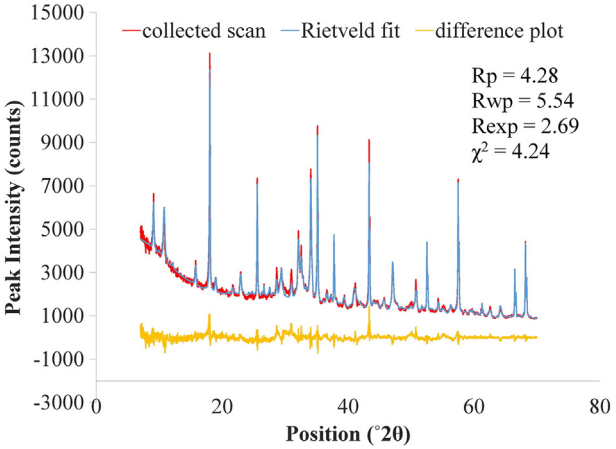


**Fig. 7.** 10MK paste sample at 7 days with 20% SRM 676a.

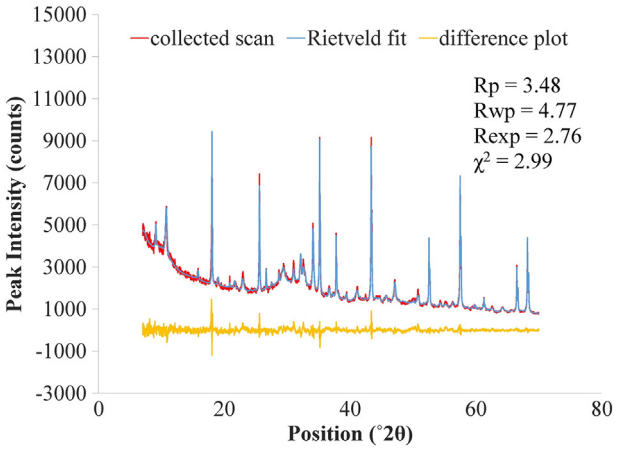


**Fig. 8.** 52SL paste sample at 7 days with 20% SRM 676a.

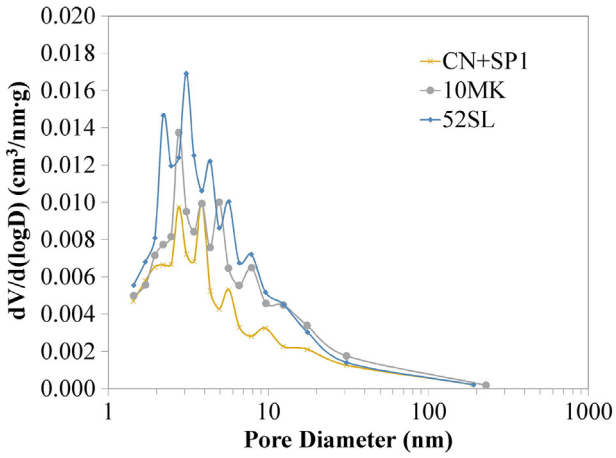


**Fig. 9.** BJH pore size distribution at 7 days.

**Table 7**
Rietveld analysis of the pastes at the age of 7 days.

| Phase | ICSD # | CN + SP1 | 10MK | 52SL |
|---|---|---|---|---|
| Alite | 94742 | 2.0 | 1.4 | 0.1 |
| Belite | 81096 | 13.9 | 13.3 | 6.0 |
| $C_3A$ | 1841 | 1.6 | 1.3 | 0.0 |
| Ferrite | 9197 | 3.0 | 1.7 | 0.0 |
| Portlandite | 15471 | 12.9 | 8.0 | 4.2 |
| Quartz | 41414 | 0.8 | 0.4 | 0.8 |
| Calcite | 80869 | 1.0 | 0.9 | 0.6 |
| Ettringite | 155395 | 8.6 | 6.6 | 3.1 |
| Tobermorite 9A | 87689 | 1.0 | 1.5 | 2.8 |
| Hemicarboaluminate | 263124 | 2.8 | 4.0 | 3.8 |
| Monocarboaluminate | 59327 | 0.4 | 0.0 | 0.0 |
| 0.8-Carboaluminate | 263123 | 0.2 | 0.0 | 0.0 |
| Amorphous/unidentified | | 51.8 | 61.1 | 78.3 |

presence of less porous CSH. The ratio of LD/HD CSH is known to affect shrinkage and creep of concrete (Jennings et al., 2008).

### 3.5. Nanoindentation

The results obtained from grid indentation were used to calculate the average elastic modulus ($E$), hardness ($H$) and average maximum depth of penetration ($h_{max}$) for each sample. First, the average $E$, $H$ and $h_{max}$ were calculated based on the data obtained from all the indents, which would include both the hydration products and the unhydrated clinker phases (Table 10). The average maximum penetration depths are very similar and indicate that the majority of the indents were made in the CSH phase (Ulm et al., 2010). However, large differences can be observed between the average elastic moduli and average hardness values for these samples. The CN + SP1 sample had the highest elastic modulus, followed by 52SL, and 10MK sample had the lowest. The average hardness of the 10MK sample was also significantly lower than that of the other samples.

The elastic modulus of individual clinker phases is known to be significantly higher than that of hydration products (Velez et al., 2001). Despite a large difference in the degree of hydration of 10MK and 52SL samples, (Table 6), their average elastic moduli are similar, while there is a large difference in the $E$ values for 10MK and CN + SP1 samples in spite of their similar degree of hydration. This indicates that the average $E$ values in Table 10 are heavily influenced by the presence of unhydrated clinker phases and may not be the best way to evaluate the mechanical properties of the hydrated paste.

In order to evaluate the influence of MK and SL addition on the average mechanical properties of the hydration products and eliminate the effect of the large difference in the degree of hydration, the average $E$, $H$, and $h_{max}$ values were recalculated excluding indents with $E > 40$ GPa (Table 11). A number of $E$ and $H$ values for CSH and CH have been reported in the literature by Constantinides and Ulm (2004), Hu and Li (2014), Hu et al. (2014), Hughes and Trtik (2004), Jennings et al. (2007), Monteiro and Chang (1995), and Pelisser et al. (2012). Němeček et al. (2011) reported a modulus of approximately 44 GPa for unreacted MK and 26 GPa for unreacted SL. Therefore, 40 GPa was selected as a cutoff point to ensure that all the possible CSH packing arrangements were included in the adjusted average values, but the unreacted MK, if any may be present in the 10MK sample, was excluded. Since the expected value for unreacted SL modulus was between those reported for LD and HD CSH, it could not be excluded. However, based on Fig. 13c it appears that minimal number of indents were made in the unreacted SL particles and they are not expected to have a significant effect on the values calculated for the 52SL sample (Table 11).

The adjusted average $E$ values in Table 11 correlate with compressive strength results (Fig. 11); compressive strength appears to increase with an increase in average elastic modulus computed for values below

**Table 8**
Consumption of individual clinker phases at the age of 7 days.

| Phase | CN + SP1 | 10MK | 52SL |
|---|---|---|---|
| $C_3S$ | 0.94 | 0.95 | 0.99 |
| $C_3A$ | 0.75 | 0.78 | 1 |
| $C_4AF$ | 0.44 | 0.65 | 1 |

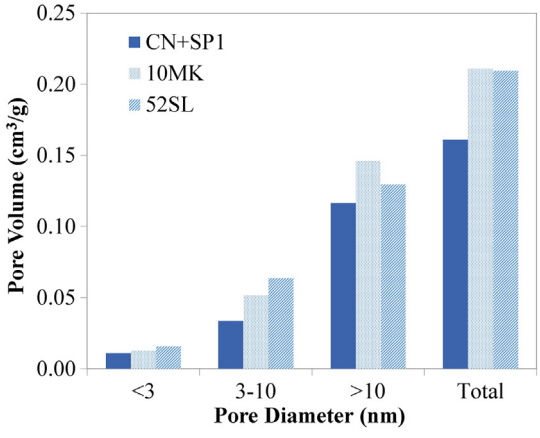


**Fig. 10.** BJH pore volumes for each paste sample at 7 days.

Please cite this article as: Shanahan, N., et al., Multi-technique investigation of metakaolin and slag blended portland cement pastes, Appl. Clay Sci. (2016), http://dx.doi.org/10.1016/j.clay.2016.07.015

**Table 9**
BET surface areas at 7 days.

| Mix ID | 5-Point BET SSA ($m^2/g$) |
|---|---|
| CN + SP1 | 53.35 |
| 10MK | 72.18 |
| 52SL | 86.37 |

**Table 10**
Average nanoindentation values.

| Sample | Average $E$ (GPa) | Average $H$ (GPa) | Average $h_{max}$ (nm) |
|---|---|---|---|
| 10MK | 19.7 | 0.5 | 323 |
| CN + SP1 | 30.1 | 1.2 | 294 |
| 52SL | 23.0 | 1.4 | 323 |

**Table 11**
Adjusted average values after excluding indentations with $E > 40$ GPa.

| Sample | Average $E$ (GPa) | Average $H$ (GPa) | Average $h_{max}$ (nm) |
|---|---|---|---|
| CN + SP1 | 21.6 | 0.5 | 327 |
| 10MK | 19.7 | 0.5 | 323 |
| 52SL | 14.7 | 0.5 | 370 |

40 GPa. Additionally, there is good agreement between the adjusted average $E$ values and porosity results, specifically LGP volume; as the LGP volume increased, the adjusted average $E$ decreased (Fig. 12a). Same trend was observed with the BET surface area as well (Fig. 12b).

Further analysis of nanoindentation data was carried out by plotting the probability distributions of the elastic moduli (below 40 GPa) for each sample (Fig. 13). The values of the elastic moduli obtained from the deconvolution analysis (Table 12) are in general agreement with the published literature (see Table 1).

The probability plot for the 10MK sample (Fig. 13b) is significantly different from that of CN + SP1 (Fig. 13a). While the control sample is showing presence of low stiffness, LD and HD CSH, the microstructure of the 10MK sample appears to be dominated by low stiffness CSH. A presence of a porous phase has also been identified in the 10MK sample. 52SL sample contained a significantly higher amount of the porous phase (Fig. 13c), and CSH morphology was dominated by low stiffness CSH with very small amount of HD CSH present. Vandamme et al. (2010) illustrated a relationship between w/c ratio and relative volumes of LD, HD and UHD CSH; as w/c ratio increases, so does the volume of LD CSH at the expense of the HD CSH. The volumes fractions of low stiffness-LD CSH observed in this study appears to be affected by the effective w/c ratios of the mixtures. Although the w/b ratio was maintained constant, the w/c ratio of the 52SL mixture was significantly higher,

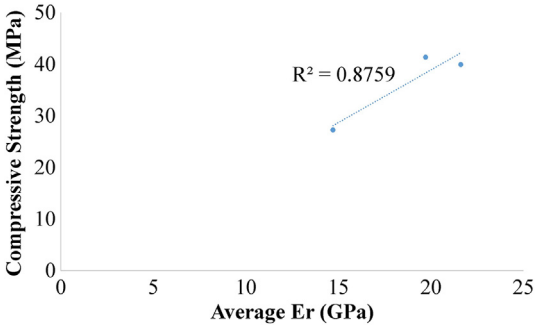


**Fig. 11.** Relationship between compressive strength and average nanoindentation modulus of hydration products at 7 days.

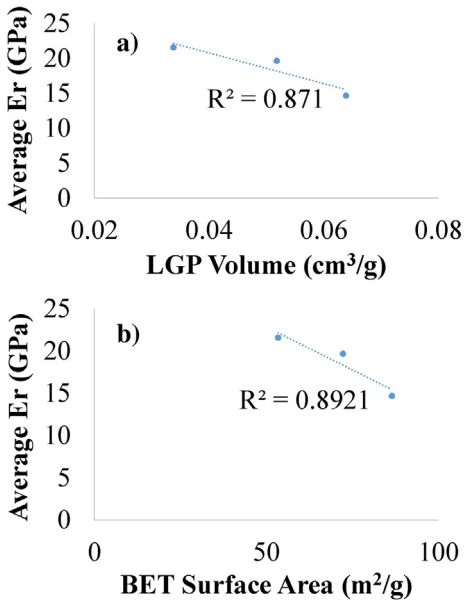


**Fig. 12.** Relationship between (a) LGP pore volume and (b) BET surface area and average nanoindentation modulus of hydration products at 7 days.

especially taking into account the low reactivity of SL compared to MK at 7 days.

There are no indents with elastic moduli in the CH range for the 52SL sample. The absence of a clear indication of CH presence by nanoindentation is not surprising, as Rietveld refinement identified minimal amounts of CH compared to the other samples. Generally, the volume fraction of CH is in agreement with the XRD results (Fig. 14). It appears that at 4 wt%, as measured by XRD analysis, CH is difficult to detect with grid nanoindentation.

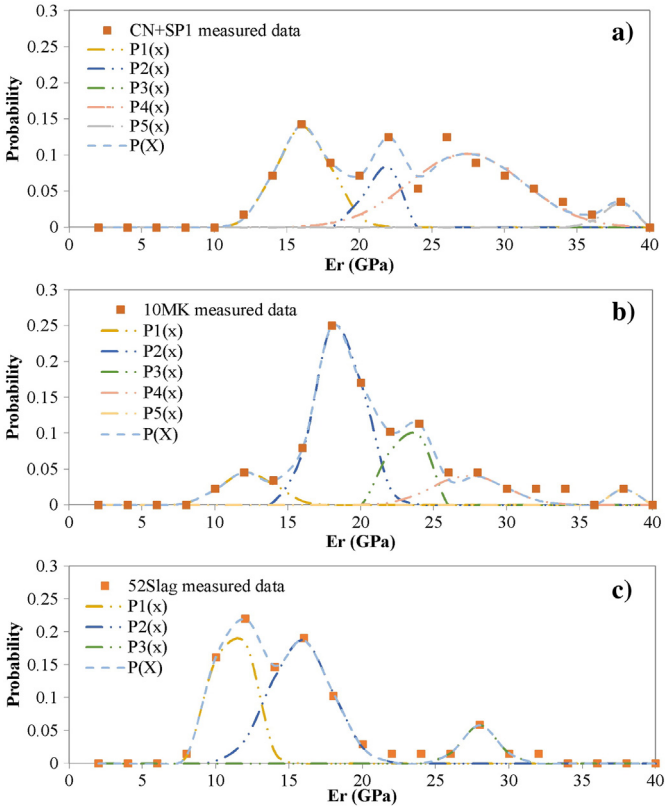


**Fig. 13.** Probability density functions of (a) control, (b) 10MK and (c) 52SL paste at 7 days.

Please cite this article as: Shanahan, N., et al., Multi-technique investigation of metakaolin and slag blended portland cement pastes, Appl. Clay Sci. (2016), http://dx.doi.org/10.1016/j.clay.2016.07.015

**Table 12**
Results of the deconvolution analysis.

| Sample | Phase | Mean ± standard deviation (GPa) | Volume fraction |
|---|---|---|---|
| CN + SP1 | Low stiffness CSH | 16.1 ± 1.9 | 0.31 |
| | LD CSH | 21.1 ± 0.6 | 0.17 |
| | HD CSH | 27.4 ± 3.9 | 0.48 |
| | CH | 37.3 ± 0.7 | 0.04 |
| 10MK | Porous phase | 12.3 ± 1.8 | 0.10 |
| | Low stiffness CSH | 18.5 ± 1.6 | 0.48 |
| | LD CSH | 23.0 ± 0.6 | 0.28 |
| | HD CSH | 27.4 ± 2.5 | 0.12 |
| | CH | 38.3 ± 0.1 | 0.02 |
| 52SL | Porous phase | 11.1 ± 1.3 | 0.39 |
| | Low stiffness CSH | 15.8 ± 2.1 | 0.52 |
| | HD CSH | 28.00 ± 1.2 | 0.09 |

## 4. Conclusions

The following conclusions can be made based on the findings of this study:

- Generally, addition of chemical and mineral admixtures did not change the main hydration products for mixtures cured at 23 °C. No significant differences in phase consumption were observed with addition of 10% metakaolin or 52% slag compared to the control paste at 7 days.
- Despite the similarity in phase consumption and the hydration products formed, nitrogen adsorption measurements indicated an increase in LGP volume with addition of 10% MK and 52% SL as well as an increase in the fraction of capillary pores accessible by nitrogen adsorption technique.
- Nanoindentation measurements also indicated an increase in CSH porosity with 10% MK and 52% SL addition, the highest increase resulting from SL incorporation which is in agreement with nitrogen adsorption measurements.
- Additionally, a linear relationship was observed between the average elastic modulus of the hydration products obtained from nanoindentation and the volume of LGP from $N_2$ adsorption. A linear relationship was also observed between the average elastic modulus and compressive strength.

The results of this study indicate that phase quantification by QXRD of hydrated pastes may not be sufficient to assess the impact of metakaolin or slag addition on hydrating cementitious systems, and a multi-technique approach that provides information not only on the amount of hydration products, but also their morphology is preferable.

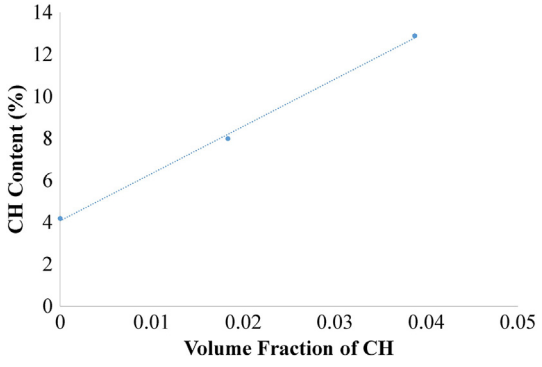


**Fig. 14.** Relationship between volume fraction of CH obtained from nanoindentation and weight percent of CH calculated from XRD measurements.

## Acknowledgements

The authors would also like to thank the Florida Department of Transportation and the Federal Highway Administration for providing partial funding for this work under contract number BDV25-977-02. The opinions, findings, and conclusions expressed in this publication are those of the authors and not necessarily those of the Florida Department of Transportation or the US Department of Transportation.

## Appendix A. Supplementary data

Supplementary data to this article can be found online at http://dx.doi.org/10.1016/j.clay.2016.07.015.

## References

Abdolhosseini Qomi, M.J., Krakowiak, K.J., Bauchy, M., Stewart, K.L., Shahsavari, R., Jagannathan, D., Brommer, D.B., Baronnet, A., Buehler, M.J., Yip, S., Ulm, F.-J., Van Vliet, K.J., Pellenq, R.-M., 2014. Combinatorial molecular optimization of cement hydrates. Nat. Commun. 5, 1–9. http://dx.doi.org/10.1038/ncomms5960.

Aligizaki, K.K., 2006. Pore Structure of Cement-based Materials: Testing, Interpretation and Requirements. Taylor & Francis, New York, NY.

Ambroise, J., Maximilien, S., Pera, J., 1994. Properties of metakaolin blended cements. Adv. Cem. Based Mater. 1, 161–168.

Antoni, M., Rossen, J., Martirena, F., Scrivener, K., 2012. Cement substitution by a combination of metakaolin and limestone. Cem. Concr. Res. 42, 1579–1589. http://dx.doi.org/10.1016/j.cemconres.2012.09.006.

Barbhuiya, S., Chow, P., 2015. Effects of metakaolin on nanomechanical properties of cement paste. In: Scrivener, K.L., Favier, A. (Eds.), Calcined Clays for Sustainable Concrete, Proceedings of the 1st International Conference on Calcined Clays for Sustainable Concrete. Springer, New York, NY, pp. 459–466 http://dx.doi.org/10.1007/978-94-017-9939-3.

Barrett, E.P., Joyner, L.G., Halenda, P.P., 1951. The determination of pore volume and area distributions in porous substances. I. Computations from nitrogen isotherms. J. Am. Ceram. Soc. 73, 373–380.

Batis, G., Pantazopoulou, P., Tsivilis, S., Badogiannis, E., 2005. The effect of metakaolin on the corrosion behavior of cement mortars. Cem. Concr. Compos. 27, 125–130. http://dx.doi.org/10.1016/j.cemconcomp.2004.02.041.

Bauchy, M., Abdolhosseini Qomi, M.J., Bichara, C., Ulm, F.J., Pellenq, R.J.M., 2014. Nanoscale structure of cement: viewpoint of rigidity theory. J. Phys. Chem. C 118, 12485–12493. http://dx.doi.org/10.1021/jp502550z.

Beaudoin, J., 2002. A discussion on, "The use of nitrogen adsorption to assess the microstructure of cement paste" by MCG Juenger and HM Jennings. Cem. Concr. Res. 32, 831–832.

Bich, C., Ambroise, J., Péra, J., 2009. Influence of degree of dehydroxylation on the pozzolanic activity of metakaolin. Appl. Clay Sci. 44, 194–200. http://dx.doi.org/10.1016/j.clay.2009.01.014.

Bish, D., Reynolds, R.J., 1989. Sample preparation for X-ray diffraction. In: Bish, D., Post, J. (Eds.), Modern Powder Diffraction. The Mineralogical Society of America, Washington, DC, pp. 73–99.

Bodor, E., Skalny, J., Brunauer, S., Massy, J., Yudenfreund, M., 1970. Pore structures of hydrated calcium silicates and Portland cements by nitrogen adsorption. J. Colloid Interface Sci. 34, 560–570.

Boháč, M., Palou, M., Novotný, R., Másilko, J., Všianský, D., Staněk, T., 2014. Investigation on early hydration of ternary Portland cement-blast-furnace slag–metakaolin blends. Constr. Build. Mater. 64, 333–341. http://dx.doi.org/10.1016/j.conbuildmat.2014.04.018.

Brunauer, S., Emmett, P.H., Teller, E., 1938. Adsorption of gases in multimolecular layers. J. Am. Chem. Soc. 60, 309–319 (doi:citeulike-article-id:4074706).

Buchwald, A., Tatarin, R., Stephan, D., 2009. Reaction progress of alkaline-activated metakaolin-ground granulated blast furnace slag blends. J. Mater. Sci. 44, 5609–5617. http://dx.doi.org/10.1007/s10853-009-3790-3.

Cassagnabère, F., Escadeillas, G., Mouret, M., 2009. Study of the reactivity of cement/metakaolin binders at early age for specific use in steam cured precast concrete. Constr. Build. Mater. 23, 775–784. http://dx.doi.org/10.1016/j.conbuildmat.2008.02.022.

Constantinides, G., Ulm, F.-J., 2004. The effect of two types of C-S-H on the elasticity of cement-based materials: results from nanoindentation and micromechanical modeling. Cem. Concr. Res. 34, 67–80. http://dx.doi.org/10.1016/S0008-8846(03)00230-8.

Constantinides, G., Ulm, F.J., 2007. The nanogranular nature of C-S-H. J. Mech. Phys. Solids 55, 64–90. http://dx.doi.org/10.1016/j.jmps.2006.06.003.

Constantinides, G., Ravi Chandran, K.S., Ulm, F.-J., Van Vliet, K.J., 2006. Grid indentation analysis of composite microstructure and mechanics: principles and validation. Mater. Sci. Eng. A 430, 189–202. http://dx.doi.org/10.1016/j.msea.2006.05.125.

Curcio, F., DeAngelis, B., Pagliolico, S., 1998. Metakaolin as a pozzolanic microfiller for high-performance mortars. Cem. Concr. Res. 28, 803–809. http://dx.doi.org/10.1016/S0008-8846(98)00045-3.

De Weerdt, K., Haha, M.B., Le Saout, G., Kjellsen, K.O., Justnes, H., Lothenbach, B., 2011. Hydration mechanisms of ternary Portland cements containing limestone powder and fly ash. Cem. Concr. Res. 41, 279–291. http://dx.doi.org/10.1016/j.cemconres.2010.11.014.

Detwiler, R., Powers, L., Jakobsen, U., Ahmed, W.U., Scrivener, K.L., Kjellsen, K.O., 2001. Preparing specimens for microscopy. Concr. Int. 23, 51–58.

Duan, P., Shui, Z., Chen, W., Shen, C., 2012. Influence of metakaolin on pore structure-related properties and thermodynamic stability of hydrate phases of concrete in seawater environment. Constr. Build. Mater. 36, 947–953. http://dx.doi.org/10.1016/j.conbuildmat.2012.06.073.

Duan, P., Shui, Z., Chen, W., Shen, C., 2013. Effects of metakaolin, silica fume and slag on pore structure, interfacial transition zone and compressive strength of concrete. Constr. Build. Mater. 44, 1–6. http://dx.doi.org/10.1016/j.conbuildmat.2013.02.075.

Gajda, J., 2007. Mass Concrete for Buildings and Bridges. Portland Cement Association, Skokie, IL.

Gluth, G.J.G., Hillemeier, B., 2012. Pore structure and permeability of hardened calcium aluminate cement pastes of low w/c ratio. Mater. Struct. 46, 1497–1506. http://dx.doi.org/10.1617/s11527-012-9991-2.

Groen, J.C., Peffer, L.A.A., Pérez-Ramírez, J., 2003. Pore size determination in modified micro- and mesoporous materials. Pitfalls and limitations in gas adsorption data analysis. Microporous Mesoporous Mater. 60, 1–17. http://dx.doi.org/10.1016/S1387-1811(03)00339-1.

Gruber, K.A., Ramlochan, T., Boddy, A., Hooton, R., Thomas, M.D.A., 2001. Increasing concrete durability with high-reactivity metakaolin. Cem. Concr. Compos. 23, 479–484. http://dx.doi.org/10.1016/S0958-9465(00)00097-4.

He, Z., Qian, C., Zhang, Y., Zhao, F., Hu, Y., 2013. Nanoindentation characteristics of cement with different mineral admixtures. Sci. China Technol. Sci. 56, 1119–1123. http://dx.doi.org/10.1007/s11431-013-5186-5.

Hemalatha, T., Gunavadhi, M., Bhuvaneshwari, B., Sasmal, S., Iyer, N.R., 2015. Characterization of micro- and nano- modified cementitious system using micro analytical techniques. Cem. Concr. Compos. http://dx.doi.org/10.1016/j.cemconcomp.2015.01.004.

Hou, D., Zhao, T., Ma, H., Li, Z., 2015. Reactive molecular simulation on water confined in the nanopores of the calcium silicate hydrate gel: structure, reactivity, and mechanical properties. J. Phys. Chem. C 119, 1346–1358. http://dx.doi.org/10.1021/jp509292q.

Hu, C., Li, Z., 2014. Property investigation of individual phases in cementitious composites containing silica fume and fly ash. Cem. Concr. Compos. http://dx.doi.org/10.1016/j.cemconcomp.2014.11.011.

Hu, C., Han, Y., Gao, Y., Zhang, Y., Li, Z., 2014. Property investigation of calcium-silicate-hydrate (C-S-H) gel in cementitious composites. Mater. Charact. 95, 129–139. http://dx.doi.org/10.1016/j.matchar.2014.06.012.

Hughes, J.J., Trtik, P., 2004. Micro-mechanical properties of cement paste measured by depth-sensing nanoindentation: a preliminary correlation of physical properties with phase type. Mater. Charact. 53, 223–231. http://dx.doi.org/10.1016/j.matchar.2004.08.014.

Ioannidou, K., Krakowiak, K.J., Bauchy, M., Hoover, C.G., Masoero, E., Yip, S., Ulm, F.J., Levitz, P., Pellenq, R.J.-M., Del Gado, E., 2016. Mesoscale texture of cement hydrates. Proc. Natl. Acad. Sci. 113, 2029–2034. http://dx.doi.org/10.1073/pnas.1520487113.

Jansen, D., Bergold, S.T., Goetz-Neunhoeffer, F., Neubauer, J., 2011a. The hydration of alite: a time-resolved quantitative XRD approach using the G-factor method compared with heat release. J. Appl. Crystallogr. 44, 895–901.

Jansen, D., Goetz-Neunhoeffer, F., Stabler, C., Neubauer, J., 2011b. A remastered external standard method applied to the quantification of early OPC hydration. Cem. Concr. Res. 41, 602–608. http://dx.doi.org/10.1016/j.cemconres.2011.03.004.

Jansen, D., Stabler, C., Goetz-Neunhoeffer, F., Dittrich, S., Neubauer, J., 2012. Does ordinary Portland cement contain amorphous phase? A quantitative study using an external standard method. Powder Diffract. 26, 31–38. http://dx.doi.org/10.1154/1.3549186.

Jennings, H.M., 2008. Refinements to colloid model of C-S-H in cement: CM-II. Cem. Concr. Res. 38, 275–289. http://dx.doi.org/10.1016/j.cemconres.2007.10.006.

Jennings, H.M., Thomas, J.J., 2004. A discussion of the paper "The BET-specific surface area of hydrated Portland cement and related materials" by Ivan Odler. Cem. Concr. Res. 34, 1959–1960. http://dx.doi.org/10.1016/j.cemconres.2004.03.001.

Jennings, H.M., Thomas, J.J., Gevrenov, J.S., Constantinides, G., Ulm, F.-J., 2007. A multi-technique investigation of the nanoporosity of cement paste. Cem. Concr. Res. 37, 329–336. http://dx.doi.org/10.1016/j.cemconres.2006.03.021.

Jennings, H.M., Bullard, J.W., Thomas, J.J., Andrade, J.E., Chen, J.J., Scherer, G.W., 2008. Characterization and modeling of pores and surfaces in cement paste: correlations to processing and properties. J. Adv. Concr. Technol. 6, 5–29.

Juenger, M.C.G., Jennings, H.M., 2002. Examining the relationship between the microstructure of calcium silicate hydrate and drying shrinkage of cement pastes. Cem. Concr. Res. 32, 289–296. http://dx.doi.org/10.1016/S0008-8846(01)00673-1.

Justice, J.M., Kurtis, K.E., 2007. Influence of metakaolin surface area on properties of cement-based materials. J. Mater. Civ. Eng. 19, 762–771. http://dx.doi.org/10.1061/(ASCE)0899-1561(2007)19:9(762).

Justice, J.M., Kennison, L.H., Mohr, B.J., Beckwith, S.L., Mccormick, L.E., Wiggins, B., Zhang, Z.Z., Kurtis, K.E., 2005. Comparison of Two Metakaolins and a Silica Fume Used as Supplementary Cementitious Materials. Proceedings of the ACI 7th International Symposium on Utilization of High- Strength/High-Performance Concrete. American Concrete Institute, Farmington Hills, MI, pp. 213–236.

Kakali, G., Perraki, T., Tsivilis, S., Badogiannis, E., 2001. Thermal treatment of kaolin: the effect of mineralogy on the pozzolanic activity. Appl. Clay Sci. 20, 73–80. http://dx.doi.org/10.1016/S0169-1317(01)00040-0.

Khatib, J., Wild, S., 1996. Pore size distribution of metakaolin paste. Cem. Concr. Res. 26, 1545–1553.

Kniess, C.T., Cardoso de Lima, J., Prates, P.B., 2012. Sintering - methods and products. In: Shatokha, V. (Ed.), Sintering - Methods and Products. InTech, pp. 293–316 http://dx.doi.org/10.5772/1305.

Korb, J.P., Monteilhet, L., McDonald, P.J., Mitchell, J., 2007. Microstructure and texture of hydrated cement-based materials: a proton field cycling relaxometry approach. Cem. Concr. Res. 37, 295–302. http://dx.doi.org/10.1016/j.cemconres.2006.08.002.

Korpa, A., Trettin, R., 2006. The influence of different drying methods on cement paste microstructures as reflected by gas adsorption: comparison between freeze-drying (F-drying), D-drying, P-drying and oven-drying methods. Cem. Concr. Res. 36, 634–649. http://dx.doi.org/10.1016/j.cemconres.2005.11.021.

Madsen, I.C., Scarlett, N.V.Y., Kern, A., 2011. Description and survey of methodologies for the determination of amorphous content via X-ray powder diffraction. Zeitschrift für Krist. 226, 944–955. http://dx.doi.org/10.1524/zkri.2011.1437.

Mehta, P.K., Monteiro, P.J.M., 2006. Concrete: Microstructure, Properties and Materials. third ed. McGraw-Hill, New York, NY.

Mikhail, R., Copeland, L.E., Brunauer, S., 1964. Pore structures and surface areas of hardened Portland cement pastes by nitrogen adsorption. Can. J. Chem. 42, 426–438.

Mindess, S., Young, J.F., Darwin, D., 2003. Concrete. second ed. Prentice Hall, Upper Saddle River, NJ.

Mondal, P., Shah, S.P., Marks, L., 2007. A reliable technique to determine the local mechanical properties at the nanoscale for cementitious materials. Cem. Concr. Res. 37, 1440–1444. http://dx.doi.org/10.1016/j.cemconres.2007.07.001.

Mondal, P., Shah, S.P., Marks, L.D., Gaitero, J.J., 2010. Comparative Study of the Effects of Microsilica and Nanosilica in Concrete. Transp. Res. Rec. J. Transp. Res. Board 2141, 6–9. http://dx.doi.org/10.3141/2141-02.

Monteiro, P.J.M., Chang, C.T., 1995. The elastic moduli of calcium hydroxide. Cem. Concr. Res. 25, 1605–1609. http://dx.doi.org/10.1016/0008-8846(95)00154-9.

Němeček, J., Šmilauer, V., Kopecký, L., 2011. Nanoindentation characteristics of alkali-activated aluminosilicate materials. Cem. Concr. Compos. 33, 163–170. http://dx.doi.org/10.1016/j.cemconcomp.2010.10.005.

Odler, I., 2003. The BET-specific surface area of hydrated Portland cement and related materials. Cem. Concr. Res. 33, 2049–2056. http://dx.doi.org/10.1016/S0008-8846(03)00225-4.

Oliver, W.C., Pharr, G.M., 1992. An improved technique for determining hardness and elastic-modulus using load and displacement sensing indentation experiments. J. Mater. Res. 7, 1564–1583.

Pecharsky, V.V.K., Zavalij, P., Zavilij, P.Y., 2009. Fundamentals of Powder Diffraction and Structural Characterization of Materials. second ed. Springer, New York, NY.

Pelisser, F., Gleize, P.J.P., Mikowski, A., 2012. Effect of the Ca/Si molar ratio on the micro/nanomechanical properties of synthetic C-S-H measured by nanoindentation. J. Phys. Chem. C 116, 17219–17227. http://dx.doi.org/10.1021/jp302240c.

Peterson, V.K., Ray, A.S., Hunter, B.a., 2006. A comparative study of Rietveld phase analysis of cement clinker using neutron, laboratory X-ray, and synchrotron data. Powder Diffract. 21, 12–18. http://dx.doi.org/10.1154/1.2040455.

Poole, J., Riding, K., Folliard, K., Juenger, M.C.G., Schindler, A.K., 2007. Hydration study of cementitious materials using semi-adiabatic calorimetry. ACI Spec. Publ. SP-241-5, pp. 59–76.

Poon, C.-S., Lam, L., Kou, S., Wong, Y.-L., Wong, R., 2001. Rate of pozzolanic reaction of metakaolin in high-performance cement pastes. Cem. Concr. Res. 31, 1301–1306. http://dx.doi.org/10.1016/S0008-8846(01)00581-6.

Poon, C.S., Kou, S.C., Lam, L., 2006. Compressive strength, chloride diffusivity and pore structure of high performance metakaolin and silica fume concrete. Constr. Build. Mater. 20, 858–865. http://dx.doi.org/10.1016/j.conbuildmat.2005.07.001.

Ramezanianpour, A.A., 2014. Metakaolin. Cement Replacement Materials. Springer Geochemistry/Mineralogy. Springer-Verlag Berlin Heidelberg, Berlin, Germany, p. 336 http://dx.doi.org/10.1007/978-3-642-36721-2.

Ramlochan, T., Thomas, M., Gruber, K.A., 2000. The effect of metakaolin on alkali–silica reaction in concrete. Cem. Concr. Res. 30, 339–344. http://dx.doi.org/10.1016/S0008-8846(99)00261-6.

Richardson, I.G., 2004. Tobermorite/jennite- and tobermorite/calcium hydroxide-based models for the structure of C-S-H: applicability to hardened pastes of tricalcium silicate, β-dicalcium silicate, Portland cement, and blends of Portland cement with blast-furnace slag, metakaol. Cem. Concr. Res. 34, 1733–1777. http://dx.doi.org/10.1016/j.cemconres.2004.05.034.

Richardson, I.G., Groves, G.W., 1992. Microstructure and microanalysis of hardened cement pastes involving ground granulated blast-furnace slag. J. Mater. Sci. 27, 6204–6212. http://dx.doi.org/10.1007/BF01133772.

Riding, K.A., Poole, J.L.J., Folliard, K.J., Juenger, M.C.G.G., Schindler, A.K., 2012. Modeling hydration of cementitious systems. ACI Mater. J. 109, 225–234.

Rodriguez, E.T., Richardson, I.G., Black, L., Boehm-Courjault, E., Nonat, A., Skibsted, J., 2015. Composition, silicate anion structure and morphology of calcium silicate hydrates (C-S-H) synthesised by silica-lime reaction and by controlled hydration of tricalcium silicate (C3S). Adv. Appl. Ceram. 114, 362–371. http://dx.doi.org/10.1179/1743676115Y.0000000038.

Scherer, G.W., 2015. Drying, shrinkage, and cracking of cementitious materials. Transp. Porous Media 110, 311–331. http://dx.doi.org/10.1007/s11242-015-0518-5.

Schindler, A.K., Folliard, K.J., 2005. Heat of hydration models for cementitious materials. ACI Mater. J. 102, 24–33.

Shanahan, N., Buidens, D., Riding, K., Zayed, A., 2016. Effect of chloride-based accelerator in the presence of water-reducing and retarding admixture on autogenous shrinkage. J. Am. Ceram. Soc. 1–12. http://dx.doi.org/10.1111/jace.14221.

Shvarzman, A., Kovler, K., Grader, G., Shter, G., 2003. The effect of dehydroxylation/amorphization degree on pozzolanic activity of kaolinite. Cem. Concr. Res. 33, 405–416. http://dx.doi.org/10.1016/S0008-8846(02)00975-4.

Siddique, R., Khan, M.I., 2011. Supplementary Cementing Materials, Engineering Materials. Springer, Berlin, Germany http://dx.doi.org/10.1007/978-3-642-17866-5.

Snellings, R., 2016. X-ray powder diffraction applied to cement. In: Scrivener, K.L., Snellings, R., Lothenbach, B. (Eds.), A Practical Guide to Microstructural Analysis of Cementitious Materials. CRC Press, Boca Raton, FL, pp. 107–176.

Snellings, R., Salze, A., Scrivener, K.L., 2014. Use of X-ray diffraction to quantify amorphous supplementary cementitious materials in anhydrous and hydrated blended cements. Cem. Concr. Res. 64, 89–98. http://dx.doi.org/10.1016/j.cemconres.2014.06.011.


Please cite this article as: Shanahan, N., et al., Multi-technique investigation of metakaolin and slag blended portland cement pastes, Appl. Clay Sci. (2016), http://dx.doi.org/10.1016/j.clay.2016.07.015

Taylor, H.F.W., 1997. Cement Chemistry. second ed. Thomas Telford Publishing, London, UK.

Toby, B.H., 2012. R factors in Rietveld analysis: how good is good enough? Powder Diffract. 21, 67–70. http://dx.doi.org/10.1154/1.2179804.

Ulm, F.J., Vandamme, M., Bobko, C., Alberto Ortega, J., Tai, K., Ortiz, C., 2007. Statistical indentation techniques for hydrated nanocomposites: Concrete, bone, and shale. J. Am. Ceram. Soc. 90, 2677–2692. http://dx.doi.org/10.1111/j.1551-2916.2007.02012.x.

Ulm, F.-J., Vandamme, M., Jennings, H.M., Vanzo, J., Bentivegna, M., Krakowiak, K.J., Constantinides, G., Bobko, C.P., Van Vliet, K.J., 2010. Does microstructure matter for statistical nanoindentation techniques? Cem. Concr. Compos. 32, 92–99. http://dx.doi.org/10.1016/j.cemconcomp.2009.08.007.

Valori, A., McDonald, P.J., Scrivener, K.L., 2013. The morphology of C–S–H: lessons from 1H nuclear magnetic resonance relaxometry. Cem. Concr. Res. 49, 65–81. http://dx.doi.org/10.1016/j.cemconres.2013.03.011.

Vandamme, M., Ulm, F.J., 2013. Nanoindentation investigation of creep properties of calcium silicate hydrates. Cem. Concr. Res. 52, 38–52. http://dx.doi.org/10.1016/j.cemconres.2013.05.006.

Van Damme, H., Pellenq, R.-M., Ulm, F.-J., 2013. Cement hydrates. In: Bergaya, F., Lagaly, G. (Eds.), Handbook of Clay Science. Elsevier, Oxford, UK.

Vandamme, M., Ulm, F.J., Fonollosa, P., 2010. Nanogranular packing of C-S-H at substochiometric conditions. Cem. Concr. Res. 40, 14–26. http://dx.doi.org/10.1016/j.cemconres.2009.09.017.

Velez, K., Maximilien, S., Damidot, D., Fantozzi, G., Sorrentino, F., 2001. Determination by nanoindentation of elastic modulus and hardness of pure constituents of Portland cement clinker. Cem. Concr. Res. 31, 555–561. http://dx.doi.org/10.1016/S0008-8846(00)00505-6.

Westphal, T., Füllmann, T., Pöllmann, H., 2009. Rietveld quantification of amorphous portions with an internal standard—mathematical consequences of the experimental approach. Powder Diffract. 24, 239–243. http://dx.doi.org/10.1154/1.3187828.

Wild, S., Khatib, J.M., Jones, A., 1996. Relative strength, pozzolanic activity and cement hydration in superplasticised metakaolin concrete. Cem. Concr. Res. 26, 1537–1544.

Wilson, W., 2013. Grinding of Cement Clinkers: Linking Multi-scale Fracture Properties to System Chemistry, Mineralogy and Microstructure (by).

Zayed, A., Shanahan, N., Tran, V., Markandeya, A., Williams, A., Elnihum, A., 2016. Effect of Chemical and Mineral Admixtures on Performance of Florida Structural Concrete. University of South Florida, Tampa, FL.

Please cite this article as: Shanahan, N., et al., Multi-technique investigation of metakaolin and slag blended portland cement pastes, Appl. Clay Sci. (2016), http://dx.doi.org/10.1016/j.clay.2016.07.015